ELSEVIER

Int. J. Therm. Sci. 41 (2002) 348–359

International Journal of Thermal Sciences

www.elsevier.com/locate/ijts

Analysis of the fluid-dynamic and thermal behaviour of a tin bath in float glass manufacturing

Manuela Prieto [a,*], José Díaz [a], Eduardo Egusquiza [b]

[a] *Energy Department, Faculty of Industrial Engineering, Oviedo University, Campus de Viesques, 33203 Gijón, Spain*

[b] *Fluid Mechanics Department, Faculty of Industrial Engineering, Politechnical University of Catalonia, Avda, Diagonal, 647 08028, Barcelona, Spain*

Received 15 February 2001; accepted 3 July 2001

Abstract

Nowadays there is increasing demand for float glass of low thickness. One of the most widely employed procedures for float glass manufacture is that proposed by Pilkington. The manufacturing of low thickness glass with the existing manufacturing units while maintaining the nominal production rates causes a loss of optical quality in the glass. As the formation of the glass ribbon in the Pilkington process takes place in a molten tin bath, it is considered that the flow and heat transfer induced in the tin bath are partially responsible for this loss of optical quality. The present paper studies the fluid-dynamics and thermal behaviour of the tin bath from both theoretical and experimental viewpoints. The study shows the existence of a flow in the opposite direction to that of the advance of the ribbon (reverse flow), whose features depend on operating conditions such us glass thickness and the manufacturer's practice of using baffles. It is also proven that the reverse flow can influence the temperatures in the molten tin bath. © 2002 Éditions scientifiques et médicales Elsevier SAS. All rights reserved.

Keywords: Glass process; Molten tin; Modelization; High temperature molten metal measurements; Finite volumes method; Convection; Lid driven flow

1. Introduction

The basic principles of float glass manufacture by the Pilkington process were proposed at the end of the nineteen sixties (Pilkington [1]). Since then, important work has been carried out to increase the quality of the product and to decrease production costs.

Nowadays there is great demand for thinner float glass and it is foreseen that this demand will increase considerably in coming years. One of the float glass applications is for car windscreens. The motor car industry is interested in reducing the weight of the car and hence it demands thinner float glass of high optical quality.

A loss of optical quality is noticed in thin glass when the nominal production rates are kept to in the existing production units (float units). Thin glass manufacturing therefore requires a decrease in the nominal production rates to avoid this decrease in optical quality.

The forming of the glass ribbon and its cooling take place in the float unit over a molten tin bath. It is believed that the flow and heat transfer induced in the tin bath by the movement of the ribbon and thermal actions are partially responsible for the loss of optical quality.

In the float process, a continuous ribbon of glass moves out of the melting furnace at a temperature higher than 1000 °C and floats along the surface of an enclosed bath of molten tin. A sketch of the float process is given in Fig. 1. The float unit is an airtight enclosure with a controlled atmosphere of nitrogen and hydrogen. The forming of the glass ribbon takes place during the passage of the glass through the float unit, where the glass is stretched to achieve the required size and exposed to cooling-heating conditions to achieve a suitable temperature for it to leave the float unit (around 600 °C). Pilkington [1] discussed the physical phenomena involved in the stretching of the glass.

The achievement of different thicknesses and widths requires the use of rollers inside the float unit, which consist of several pairs of refrigerated cylinders, which press the upper part of the ribbon edges and establish the ribbon velocity. Downstream, extraction rollers placed at the end of the float unit drag along the ribbon. A stretching model is due to Narayanaswamy [2].

Fig. 2 shows a vertical section of the float unit with the glass ribbon, the molten tin bath and the float unit atmosphere, which is continuously renewed. In addition, there

* Correspondence and reprints.
E-mail address: namuelap@correo.uniovi.es (M. Prieto).

1290-0729/02/$ – see front matter © 2002 Éditions scientifiques et médicales Elsevier SAS. All rights reserved.
PII: S1290-0729(02)01325-X

Nomenclature

A	tin bath top area	m^2
A_s	surrounding area of the tin bath surface	m^2
D	sphere diameter of the velocity meter	m
H	depth of the velocity measurement point	m
H_1	bath depth	m
L	characteristic length (Eq. (6)): plate area/plate perimeter	m
Nu_L	Nusselt number $= hL/k_a$	
Ra_L	Rayleigh number $= \beta_a(T - T_\infty)gc_{pa}L^3\rho_a^3/\mu_a^2k_a$	
T	temperature	K
$\overline{T}$	mean of temperatures measured on a line y_i	K
c_p	specific heat at constant pressure of the molten tin	$J{\cdot}kg^{-1}{\cdot}K^{-1}$
d	rod diameter of the velocity meter	m
g	gravitational acceleration	$m{\cdot}s^{-2}$
h	convective heat transfer coefficient	$W{\cdot}m^{-2}{\cdot}K^{-1}$
k	thermal conductivity of molten tin	$W{\cdot}m^{-1}{\cdot}K^{-1}$
p	pressure	Pa
q	heat flux	$W{\cdot}m^{-2}$
s	standard deviation of temperatures measured on a line y_i	K
u, v, w	velocity components in the x, y, z directions, respectively	$m{\cdot}s^{-1}$
x	coordinate along bath height	m
x_i	section representing horizontal plane	
y	coordinate along bath semi-width (from its centre)	m
y_i	measurement line	
z	coordinate along bath length	m
z_i	section representing vertical plane	

Greek symbols

β	coefficient of volumetric expansion	K^{-1}
δ	thickness of materials in the bath wall	m
ε	emissivity	
μ	dynamic viscosity of molten tin	$kg{\cdot}m^{-1}{\cdot}s^{-1}$
ρ	density of molten tin	$kg{\cdot}m^{-3}$
σ	Stefan–Boltzmann constant $= 5.67 \times 10^{-8}\ W{\cdot}m^{-2}{\cdot}K^{-4}$	

Subscripts

a	air
c	calculated
e	effective, experimental
i	index
n	number of materials in the wall
p	at constant pressure
r	radiation
s	surroundings inside the float unit
t	liquid tin
w	wall
∞	reference, ambient

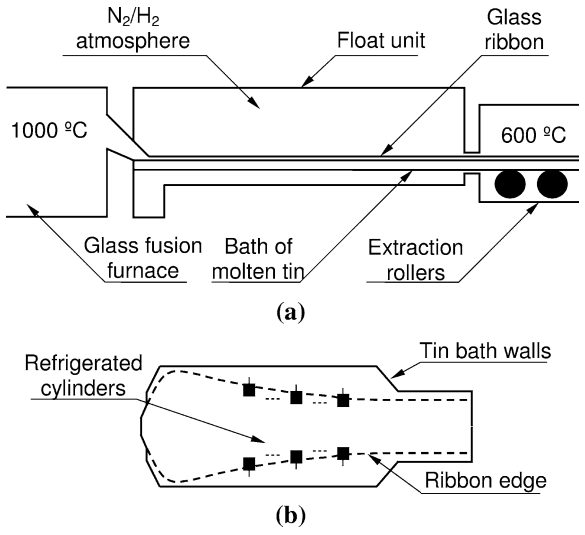

Fig. 1. Sketch of the float process: (a) vertical section, and (b) horizontal view.

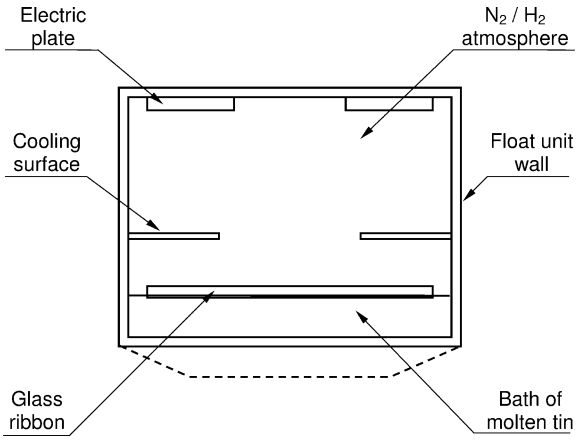

Fig. 2. Vertical section of the float unit.

are the walls: vertical side walls in contact with tin, vertical side walls in contact with the atmosphere, bottom wall and top wall and the cooling-heating temperature control elements: cylindrical cooling surfaces and electrically heated plates.

Traditionally it has been assumed that the molten tin particles linked to the surface of the ribbon caused reverse flows in the thin bath (currents in the opposite direction to that of the ribbon advance) as they were separated from the glass at the float unit outlet. The reverse flow will

be cooler than the tin flow in the direction of the ribbon advance and this could lead to inappropriate temperatures for the formation and cooling of the ribbon. However, the velocities and temperatures inside the tin bath have not nearly been measured nor theoretically calculated. Neither are the temperature changes inside the tin bath known for thinner float glass manufacturing.

This problem has a certain similitude with the lid driven cavity problem that was first experimentally investigated by Pan and Acrivos [3], and the following visualization studies by Koseff and Street [4]. However, several differences can be appreciated, such as the fact that there is a free surface at both sides outside of the ribbon glass, the particular geometry of the tin bath and the nature of the fluid.

Experimental studies are very limited, since there are difficulties with the taking of measurements. For instance, wide temperature range (from 600 °C at the coldest points to 1000 °C at the hottest ones), low accessibility to measurement points and measurement in working airtight float units (where any perturbation might seriously damage the glass). With regard to the thermal study, there are no experimental temperature measurements inside the tin bath, nor any theoretical thermal model.

The aim of this research work is to study the flow inside the tin bath taking into consideration thinner float glass manufacture and the manufacturer's practice of using baffles in the tin bath to diminish the reverse flow of the tin. So theoretical and experimental research has been undertaken to analyse the behaviour of the tin bath, from both the fluid-dynamic and thermal viewpoints. The achievement of an appropriate optical quality for thinner float glass while maintaining the nominal rates of float units was pursued.

From the theoretical point of view, the task was the development of a model to study the fluid-dynamic and thermal behaviour of the tin bath. From the experimental point of view, velocity and temperature measurements were obtained.

2. Numerical model

The usual size of the bath is between 50 and 60 m long, between 6 and 9 m wide (at the widest stage) and between 50 and 100 mm high. Fig. 3 displays a scheme of the geometry of the tin bath used in the study and the co-ordinate system (henceforth, the tin bath figures will only represent half of the horizontal view because of the symmetry through plane $y = 0$). The dashed line shows the glass ribbon edge. The governing equations for the tin bath, for the three-dimensional approach, for variable temperature properties and for negligible viscous dissipation effects in the energy equation are as follows:

Continuity:

$$\nabla \cdot \rho \boldsymbol{V} = 0 \tag{1}$$

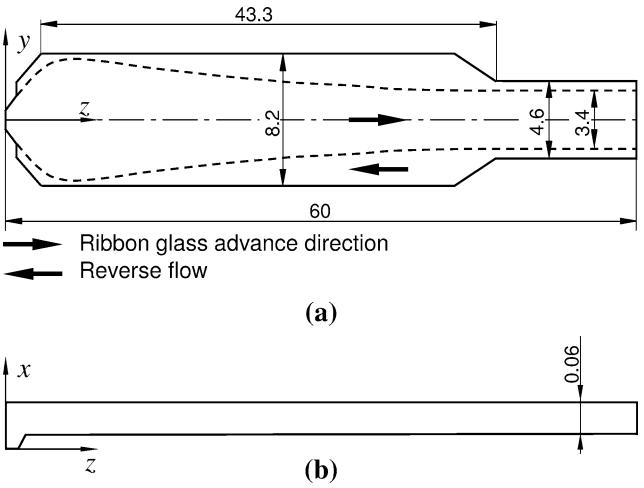

Fig. 3. Geometry of the tin bath and coordinate system: (a) horizontal view, and (b) vertical view.

Momentum:

$$\rho \boldsymbol{V} \cdot \nabla \boldsymbol{V} = \nabla \cdot \mu_{\mathrm{e}} \nabla \boldsymbol{V} - \nabla p + (\rho - \rho_{\infty}) \boldsymbol{g} \tag{2}$$

Energy:

$$\rho c_{\mathrm{p}} \boldsymbol{V} \cdot \nabla T = \nabla \cdot k \nabla T \tag{3}$$

The prescribed effective-viscosity turbulent flow model was used. This model is based on the so-called "effective-viscosity hypothesis", usually attributed to Boussinesq in 1877. The effective viscosity that best approximated the experimental measurements was $80 \cdot \mu$. When the effective viscosity was increased further than $80 \cdot \mu$, no appreciable differences were found in the resulting velocity and temperatures distributions.

Table 1 shows the values of the properties used to obtain the functions for the model solution. The boundary conditions in the tin were:

- The velocity components at the tin bath walls were established as equal to zero ($u = v = w = 0$).
- The manufacturer's expected velocity of the tin particles in contact with the ribbon along the float unit (the glass ribbon being considered to be of constant thickness along z-axis). The tin particles in contact with the ribbon followed the glass ribbon velocity profile, represented in Fig. 4(a), which is a function of z. The dashed line corresponds to a velocity profile for a 3 mm ribbon glass final thickness and the solid line corresponds to a velocity profile for a 2 mm ribbon glass final thickness.
- Negligible stress effects were applied at the free surface of the tin beyond sides of the glass, since the bath is in a controlled atmosphere and velocities are low.
- The free surface of the tin is submitted to radiation from the side walls in contact with the atmosphere, the top wall, the cooling surfaces and the electric plates. Eq. (4) from results of the method of enclosure analysis as outlined by Siegel and Howell [5] was used to estimate the heat transfer flux due to radiation at the free surface of

Table 1
Properties of the molten tin

T (K)	ρ (kg·m^{-3})	μ (kg·m^{-1}·s^{-1})	c_p (J·kg^{-1}·K^{-1})	k (W·m^{-1}·K^{-1})
516	6969.7	1.80×10^{-3}	250	34.2
676	6854.9	1.34×10^{-3}	250	33.2
873	6714.3	1.06×10^{-3}	250	32.0
971	6644.5	9.6×10^{-4}	250	31.4
1273	6428.6	8.1×10^{-4}	250	29.5

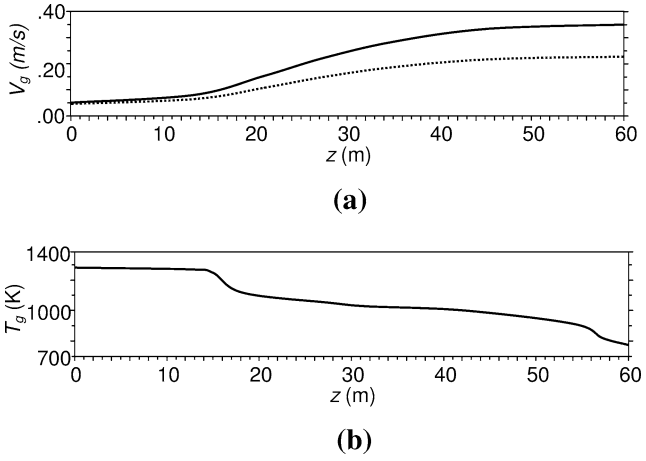

Fig. 4. Profiles of: (a) velocity, and (b) temperature of the glass ribbon along the tin bath.

the tin beyond sides of the glass. It was considered that the tin was surrounded by an imaginary surface with the same thermal properties as those produced by the real thermal elements participating in the heat exchanger. This equation depends on parameters T_s and ε_s, which were adjusted considering the results of the model of the tin bath presented in the paper, and the thermal heat transfer balances in the float unit together with temperature measurements in several zones, Prieto [6]: the float unit outer wall, the inside atmosphere of the float unit, the tin surface and the ribbon glass surface. The resulting values were maintained through all the simulations being: $T_s = 500$ K and $\varepsilon_s = 0.39$. The value of the tin emissivity was taken as $\varepsilon_t = 0.08$.

$$\dot{q}_r = \frac{\sigma}{A/A_s(1/\varepsilon_s - 1) + 1/\varepsilon_t}\left(T_s^4 - T^4\right) \tag{4}$$

- The temperature of the tin particles in contact with the ribbon along the float unit followed the glass ribbon temperature profile, represented in Fig. 4(b), which is a function of z.
- At the walls and, the heat flow rate followed Eq. (5), which was complemented by the free convection heat transfer coefficient, which was calculated from Eq. (6), suggested by McAdams [7] and Goldstein et al. [8]. The walls materials thicknesses and conductivities were: $\delta_1 = 10$ mm, $k_1 = 46.9$ W·m^{-1}·K^{-1}, $\delta_2 = 3$ mm, $k_2 = 43.5$ W·m^{-1}·K^{-1}, $\delta_3 = 305$ mm, $k_3 = 1.1$ W·m^{-1}·K^{-1}.

$$\dot{q}_w = \frac{1}{1/h + \sum_{i=1}^{n} \delta_i/k_i}(T_\infty - T) \tag{5}$$

$$Nu_L = 0.27 Ra_L^{1/4}, \qquad 3 \times 10^5 < Ra_L < 3 \times 10^{10} \tag{6}$$

The partial differential equations were discretized on a non-uniform grid using a control volume formulation (Patankar [9]). The model was solved using PHOENICS computer code (Spalding [10]) version 2.2.2 (PHOENICS [11]) and was run on an HP9000 C180 workstation under UNIX.

In order to ensure grid independence, several tests were carried out, varying the number of divisions with respect to the x, y and z axes. The results led to the adoption of a final grid of $18 \times 30 \times 80$ for the bath without baffles, which is shown in sections by an horizontal plane and by the symmetry plane in Fig. 5. Additional simulations were performed for the bath with six baffles in the zone between the glass ribbon edge projection and the vertical walls of the float unit with baffles. Fig. 6 shows the baffles arrangement and their geometry. The baffles presented a right angle corner and approach the ribbon glass as near as possible so as to diminish the reverse flow between the glass ribbon edge projection and the vertical wall of the float unit. In these simulations the number of divisions near the baffles was increased but the results did not change.

The model uses the slab-wise technique and the SIMPLEST algorithm, described by Spalding [12], in order to solve the governing equations. Linear under-relaxation was used for temperature and pressure, and false-time-step under-relaxation for the velocities.

Several conditions were specified to ensure a converged solution. The first was that the order of magnitude of the normalized residuals of pressures, velocities and temperatures diminished by four with respect to the initial ones. The second one was that there were no appreciable variations (less than 1%) in the variable values in a selected cell over an interval of 1000 iterations. Finally, the last requirement was that the energy imbalance over the whole domain was less than 0.1%.

3. Results and discussion

Simulations were performed using the model for the geometries shown in Figs. 5 and 6. Fig. 6(a) shows sections representing vertical planes perpendicular to the symmetry plane of the bath $y = 0$: (z_1, z_2, z_4 and z_6) for the theoretical study and (z_3, z_5) for the experimental study. Fig. 6(b) shows

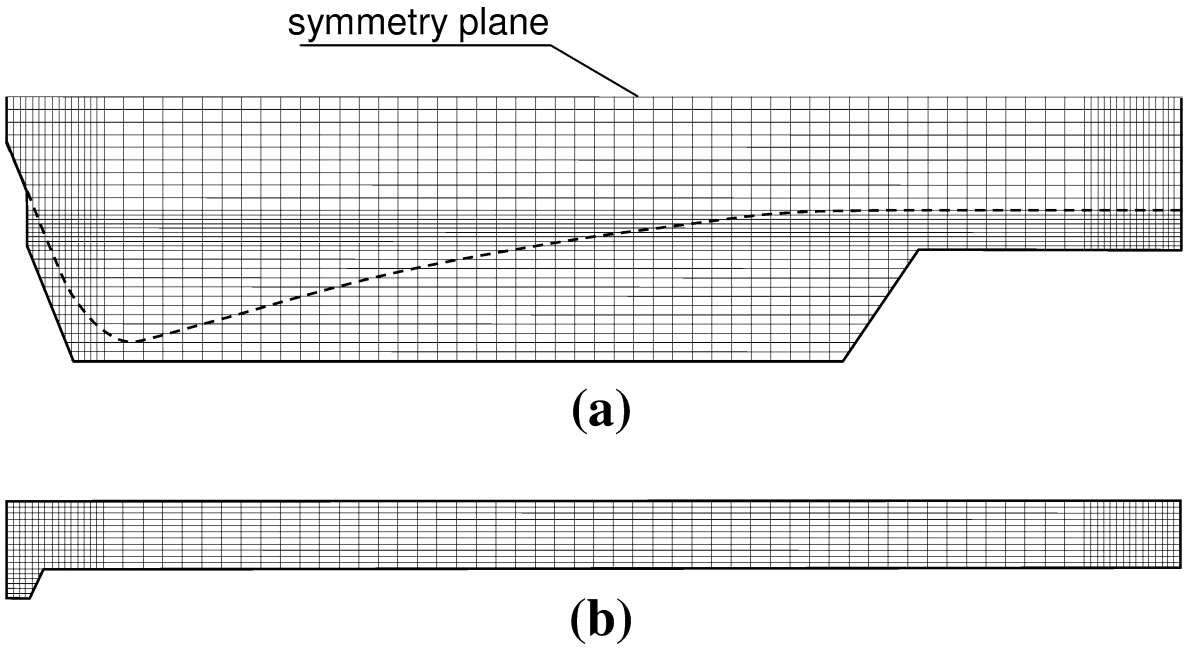

Fig. 5. Tin bath grid: (a) horizontal view, and (b) vertical view at the symmetry plane.

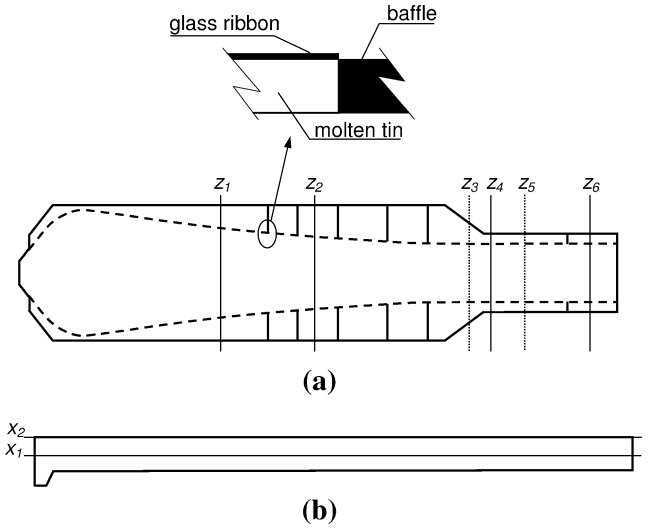

Fig. 6. Geometry, baffles arrangement and bath sections used in the study: (a) horizontal view, and (b) vertical view.

sections representing horizontal planes for the theoretical study (x_1 and x_2).

Simulations were performed for the bath without baffles and the bath with baffles for the two glass ribbon velocity profiles showed in Fig. 4(a). Both velocity profiles lead to the same glass mass flow rate, 5.9 kg·s^{-1}. The resulting velocity and temperature fields were obtained for all the simulations. A scale factor was used in this representation, namely, the position values for the x-axis were multiplied by 12 in order to be able to see the contours. The real bath is 60 mm high approximately and the semi-width is 2.3 to 4.1 m. By comparing results, it is possible to study the effect of introducing baffles and of the velocity profiles, these latter being related to the production of thinner glass, while at the same time maintaining production rates.

3.1. Bath without baffles

3.1.1. Final thickness 3 mm

The velocity vectors through the horizontal plane that is placed in the middle of the bath ($x = x_1$) are presented in Fig. 7(a). There is an important reverse flow in the narrowest zone between the glass ribbon edge projection and the vertical wall of the float unit at the end of the tin bath. The maximum calculated velocity approaches the velocity imposed for tin in contact with the glass ribbon as boundary condition, which is 0.23 m·s^{-1}. In the zone where the tin bath gets wider, the reverse flow near the glass ribbon is unimportant, but increases as it reaches the vertical wall. Near the beginning of the bath, the reverse flow diminished as expected. Under the glass ribbon it can be appreciated that the velocity has the same direction as the glass ribbon movement but the values are very low since the effect of the glass ribbon drag force at this level is low. But sections representing a horizontal plane below that corresponding to x_1 presented an important reverse flow in this zone.

The velocity vectors through the horizontal plane very near the surface ($x = x_2$) presented in Fig. 7(b) are similar in appearance to those of Fig. 7(a) between the glass ribbon edge projection and the vertical wall of the float unit. However, the velocities in the reverse flow are lower for the narrow zone of the bath and in the zone where the tin bath gets wider, velocities with the same sense as the glass ribbon advance can be appreciated as a result of the influence of the glass ribbon. Moreover, velocity vectors under the glass ribbon have the same direction as the glass ribbon movement

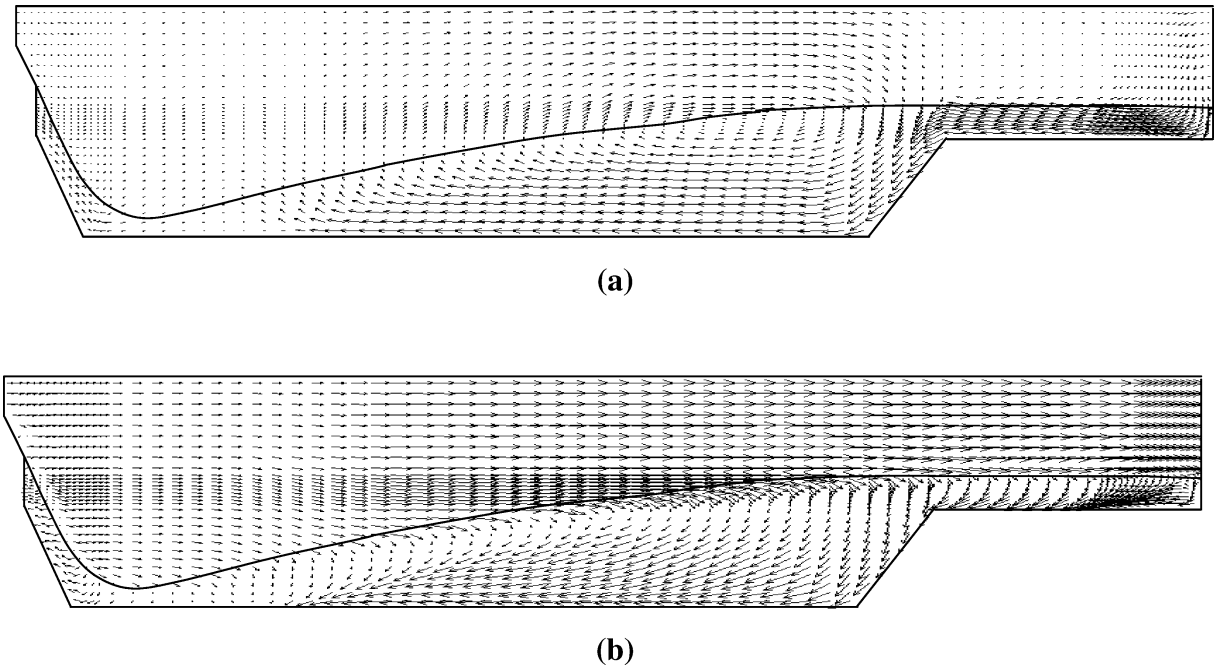

Fig. 7. Velocity vectors for the tin bath without baffles and 3 mm ribbon thickness through: (a) horizontal plane $x = x_1$, and (b) horizontal plane $x = x_2$.

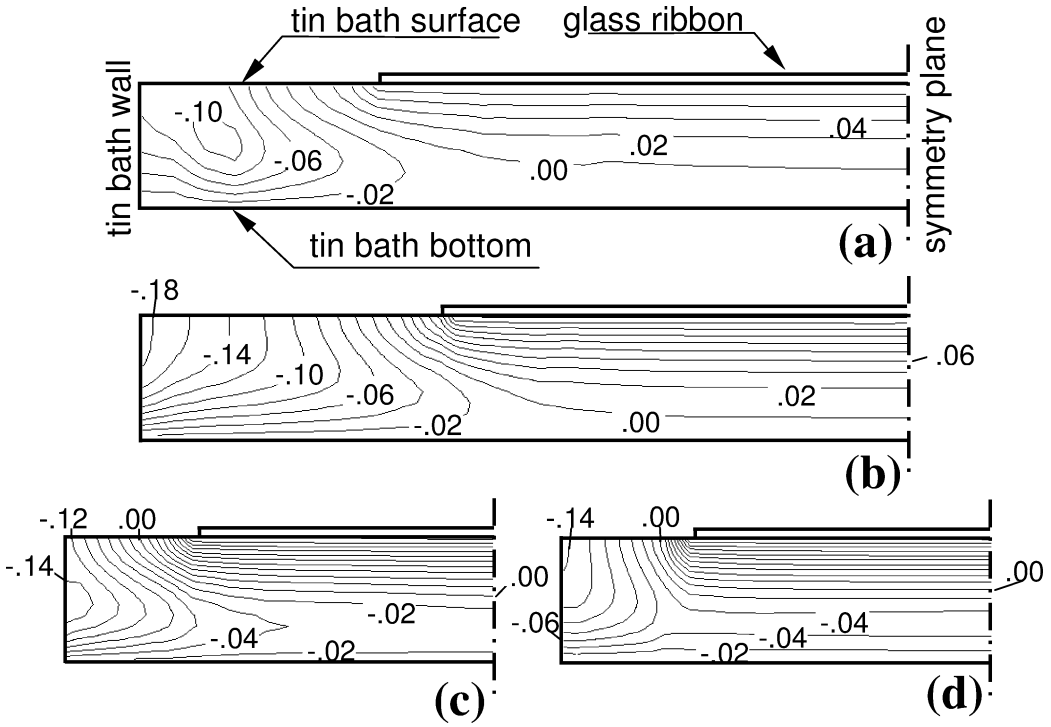

Fig. 8. Velocity contours (w, m·s^{-1}) for the tin bath without baffles and 3 mm ribbon thickness in sections: (a) $z = z_1$, (b) $z = z_2$, (c) $z = z_4$, and (d) $z = z_6$.

and the values when approaching the end of the tin bath are close to those imposed as boundary condition for tin in contact with the glass ribbon.

Fig. 8 shows the velocity contour at $z =$ constant sections and confirms the results of Fig. 7. It can be appreciated that there is an important reverse flow along the tin bath between the glass ribbon edge projection and the vertical wall of the float unit and the maximum velocity between the glass ribbon edge projection and the vertical wall of the float unit is generally near the tin surface. Under the glass ribbon in the widest zone of the tin bath, sections (a) and (b) the flow essentially follows the direction of the ribbon movement, but a reverse flow can also be appreciated in the narrowest zone, sections (c) and (d).

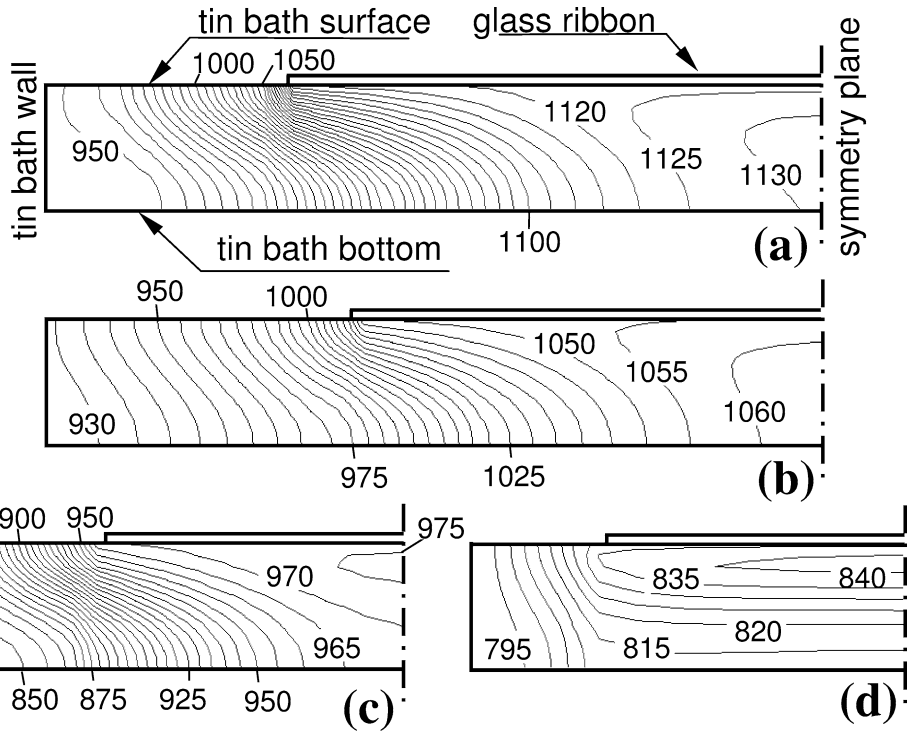

Fig. 9. Temperature contours (T, K) for the tin bath without baffles and 3 mm ribbon thickness in sections: (a) $z = z_1$, (b) $z = z_2$, (c) $z = z_4$, and (d) $z = z_6$.

Fig. 9 presents the temperature contours at $z =$ constant section. As a result of the scale factor, the isotherms, which appear in Fig. 9, are deformed. A real representation of the temperature contours between the glass ribbon edge projection and the vertical wall of the float unit showed that the isotherms were practically horizontal and that near the bottom wall the slope of the curves changed slightly towards the vertical. This behavior is due to the high transfer rate from the free surface compared with the heat transfer rate from the walls. The temperature gradient diminishes under the glass ribbon zone as the symmetry plane is approached at section (a) and (b), but higher temperature gradients are observed for section (c) and (d) and the isotherms are nearly horizontal at section (d). The behavior in the reverse flow under the glass ribbon might be explained by the low velocities in the beginning of the bath, which approach zero, compared to the velocities at the end of the bath, which are appreciably greater.

3.1.2. Final thickness 2 mm

The general appearance of the velocity vectors through horizontal planes was similar to that obtained for the 3 mm thickness. There was an important reverse flow between the glass ribbon edge projection and the float unit vertical wall all along the tin bath and the calculated values are greater than for 3 mm. The velocity contours showed that the maximum velocity values for the reverse flow between the glass ribbon edge projection and the float unit vertical wall were situated near the surface or in the middle of the zone. However, the velocities increased as the thickness decreased to 2 mm (higher ribbon velocity). The maximum velocity values for the reverse flow were 0.16 $m{\cdot}s^{-1}$, 0.24 $m{\cdot}s^{-1}$, 0.20 $m{\cdot}s^{-1}$ and 0.18 $m{\cdot}s^{-1}$ for sections (a), (b), (c) and (d), respectively. These represent an increase in velocity respect the results for 3 mm thickness of 0.06 $m{\cdot}s^{-1}$ for the first three sections and of 0.04 $m{\cdot}s^{-1}$ for the last one.

The temperature contours presented also a similar appearance as for the 3 mm thickness. The minimum temperature between the glass ribbon edge projection and the vertical wall of the float unit decreased 10 K with respect to those calculated for the 3 mm thickness at sections (a), (c) and (d). Meanwhile, at section (b) the minimum temperature between the glass ribbon edge projection and the vertical wall of the float unit decreased 5 K with respect to the values calculated for the 3 mm thickness. Under the glass ribbon the minimum value of temperature increased more or less 5 K. Therefore, the temperatures in the reverse flow were lower between the glass ribbon edge projection an the vertical wall and, in general, the temperature gradient increased appreciably.

3.2. Bath with baffles

3.2.1. Final thickness 3 mm

The velocity vectors through the horizontal plane that is placed in the middle (x_1) are presented in Fig. 10(a). There are vortices between baffles between the glass ribbon edge projection and the float unit vertical wall all along the tin bath. Moreover, substantial velocity values are still appreciated in the reverse flow direction in the narrowest zone of the tin bath. Between baffles in the widest zone of the tin bath, the velocities calculated in the reverse flow direction

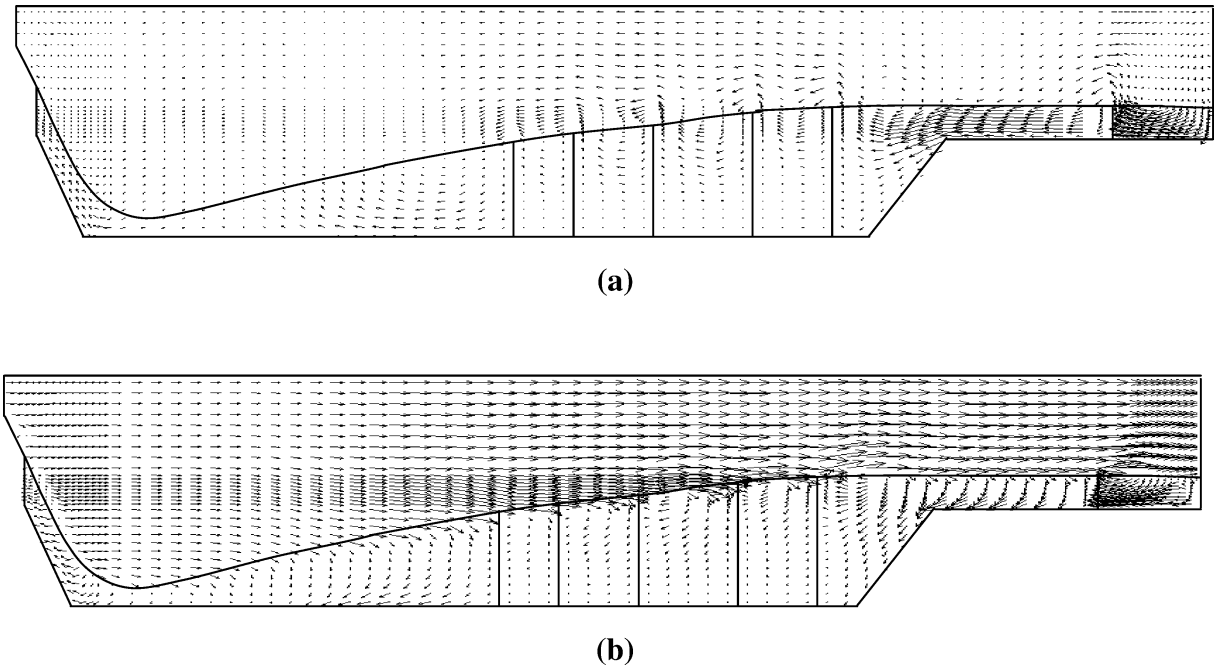

Fig. 10. Velocity vectors for the tin bath with baffles and 3 mm ribbon thickness through: (a) horizontal plane $x = x_1$, and (b) horizontal plane $x = x_2$.

are lower than for the bath without baffles. This confirms the utility of using baffles to diminish the reverse flow.

The velocity vectors through the horizontal plane near the surface (x_2) in the zone between the glass ribbon edge projection and the vertical wall of the float unit, presented in Fig. 10(b), are similar in appearance to those of Fig. 10(a). Velocities with the same direction as the glass ribbon advance are very low between the glass ribbon edge projection and the float unit vertical wall.

Fig. 11 presents the velocity contours at $z =$ constant sections. It can be appreciated that there is an important reverse flow between the glass ribbon edge projection and the vertical wall of the float unit at sections (c) and (d), which are situated in the narrowest zone of the bath. This reverse flow corresponds to the large vortex already mentioned in Fig. 10. At sections (a) and (b) in the widest zone of the bath, low velocities were calculated between the glass ribbon edge projection and the vertical wall of the float unit. A return flow is observed under the glass ribbon at section (b), which corresponds to a vortex placed between baffles that was not observed in the bath without baffles.

Fig. 12 shows the temperature contours. Sections (c) and (d) are similar in appearance to those of the tin bath without baffles. The temperature gradients obtained for section (d) are equal to those observed in the bath without baffles. However, the temperature gradients for section (c) are slightly lower than for the bath without baffles. Sections (a) and (b) are very different to those of the bath without baffles and the temperature gradients are appreciably lower due to the vortices obtained from simulation in the narrowest zone of the bath.

3.2.2. Final thickness 2 mm

The general appearance of the velocity vectors through horizontal planes was similar to that obtained for the 3 mm thickness. There were vortices between baffles and substantial velocity values in the reverse flow direction were calculated between the glass ribbon edge projection and the vertical wall of the float unit at the end of the tin bath and in the zone where the tin bath gets wider. The velocities calculated between baffles in the wider zone in the reverse flow direction are low. As with the bath without baffles, the reverse velocity values increased when the thickness decreased to 2 mm. The maximum velocity values for the reverse flow were 0.08 $m{\cdot}s^{-1}$, 0.08 $m{\cdot}s^{-1}$, 0.20 $m{\cdot}s^{-1}$ and 0.16 $m{\cdot}s^{-1}$ for sections (a), (b), (c) and (d), respectively. Sections (a) and (b) thus present similar values, while at section (c) the maximum velocity in the reverse flow increased 0.06 $m{\cdot}s^{-1}$, and at section (d) the maximum velocity in the reverse flow increased 0.02 $m{\cdot}s^{-1}$.

The temperature contours also presented a similar appearance to those for the 3 mm thickness. However some differences were observed with respect to the calculated temperatures. The minimum temperature between the glass ribbon edge projection and the float unit vertical wall increased 5 K at section (a). The calculated temperatures coincided at section (b). While at sections (c) and (d), the minimum of temperature decreases 5 K.

4. Experimental results

Measurement of the velocities inside the tin bath was difficult due to the high temperatures in the bath and the requirement of taking measurements in a working

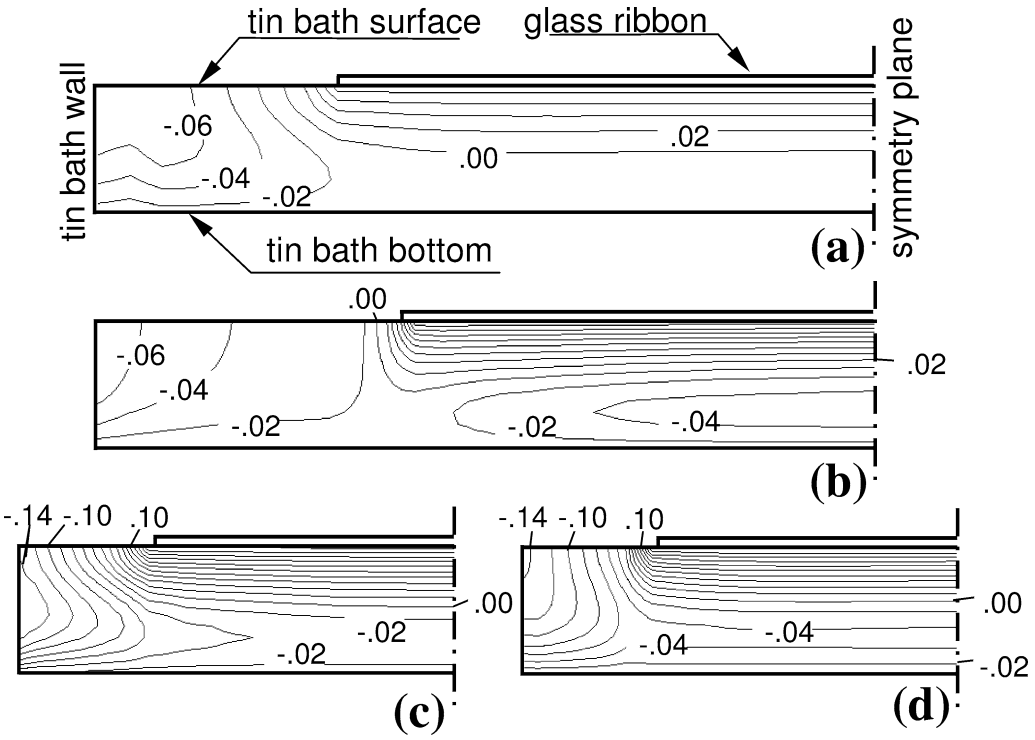

Fig. 11. Velocity contours (w, m·s^{-1}) for the tin bath with baffles and 3 mm ribbon thickness in sections: (a) $z = z_1$, (b) $z = z_2$, (c) $z = z_4$, and (d) $z = z_6$.

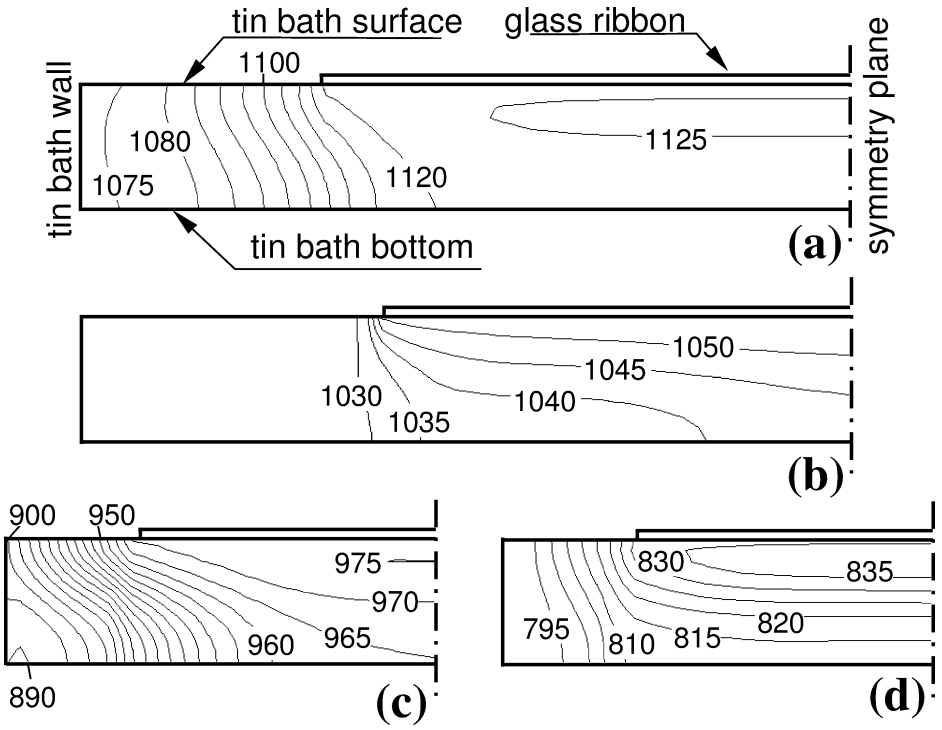

Fig. 12. Temperature contours (T, K) for the tin bath with baffles and 3 mm ribbon thickness in sections: (a) $z = z_1$, (b) $z = z_2$, (c) $z = z_4$, and (d) $z = z_6$.

airtight float (inlet air reacts with the molten tin, producing impurities in the glass). A specially designed meter was used, as there was no commercial meter for working inside the tin bath in the airtight float unit at high temperatures. The underlying basis of this meter and its calibration were presented in Prieto [13]. The estimated velocity uncertainty being ± 0.005 m·s^{-1} when the meter is used with liquid tin and the properties are evaluated at a temperature of 873 K.

The measurement principle of the meter was based on the drag force caused by fluids on submerged bodies. The

submerged body (sensing element) was a sphere. This shape was chosen because its drag coefficient was not altered by changes in the flow direction. The diameter, D of the sphere was studied theoretically as a function of the expected velocity range while bearing in mind the geometrical and physical limiting factors of the tin bath, as a result a value of 20 mm was taken. Fig. 13 shows the main geometrical variables of the device taken into account. This meter measures w (velocity component with respect to z) by obtaining the force acting on the sphere surface in the z direction, and was calibrated for a bath depth H_1, from 50 mm to 100 mm. To transmit the force outside the float unit, the sphere was linked to a vertical rod (diameter $d = 1.5$ mm) and the sphere-rod arrangement was coupled to a horizontal, thin bar by means of a rigid coupling. Outside the float unit, the force was transmitted to a load cell, which measured the torque while preventing the bar turning upwards; the force and subsequently the velocity being calculated from this measurement.

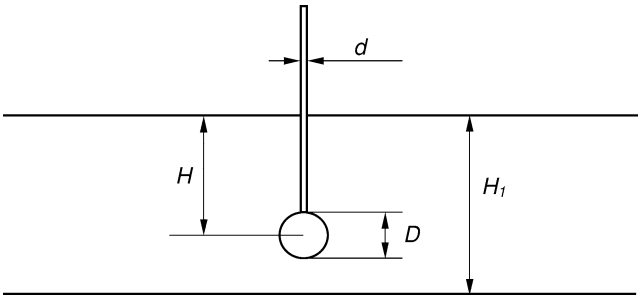

Fig. 13. Main geometrical variables of the measurement device, where $d = 1.5$ mm and $D = 20$ mm.

4.1. Velocity measurement

Velocity measurements were taken in the tin bath for a float unit during the production process at points corresponding to sections $z =$ constant planes. Section positions were decided according to accessibility criteria. The measurement points at each section were placed in the zone between a vertical line passing through the ribbon edge and the float unit wall. It was not possible to measure under the glass ribbon because the designed velocity meter was not suitable for taking measurements at these points. Besides, approaching the glass too closely could be very hazardous for the formation of the ribbon.

The following criteria were used to validate the model: velocity contours for the w velocity component at $z =$ constant sections and analysis of this component velocity values obtained at each section. The data were obtained for a glass ribbon of 2 mm thickness using the bath geometry and the baffles geometry and arrangement of Fig. 6.

Fig. 14 shows the velocity contours for the section $z = z_3$, which was in the zone where the tin bath gets wider; Fig. 14(a) representing the model results and Fig. 14(b), the experimental results. Contour lines, as well as velocity values, are similar and the flow pattern is attributed to the formation of a vortex, with the vortex vector pointing upwards.

Fig. 15 corresponds to the results at the section $z = z_5$, which was in the narrowest zone of the bath. The results for the theoretical model are presented in Fig. 15(a), whereas the experimental results are to be seen in Fig. 15(b). There is quite good agreement between both results: the velocities are close to the calculated ones and the contour lines are

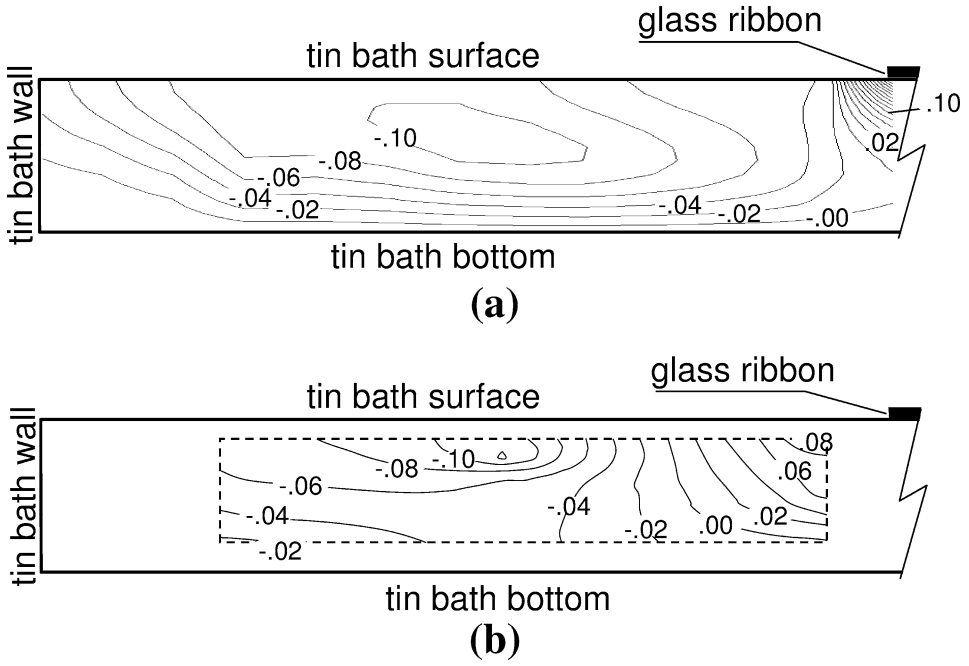

Fig. 14. Velocity contours (w, m·s^{-1}) for a tin bath with baffles and 2 mm ribbon thickness in section $z = z_3$ from: (a) model results, and (b) measurement results.

also quite similar. Inspection of Fig. 10 can lead to the interpretation of these results. The section is situated in a zone where there is an important vortex, which extends from the baffle in the narrowest zone to the baffle in the widest zone, the vortex vector pointing upwards. Comparing the results of both sections, it can be appreciated that the velocity values at section $z = z_5$ are greater than those at section $z = z_3$.

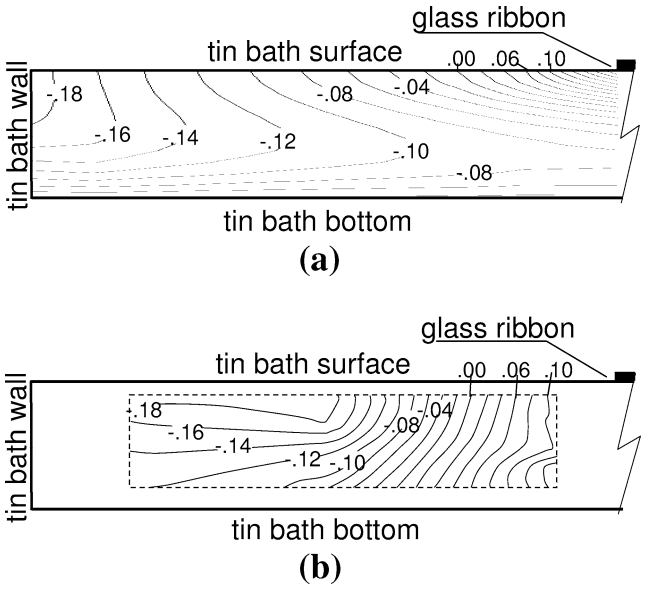

Fig. 15. Velocity contours (w, m·s^{-1}) for a tin bath with baffles and 2 mm ribbon thickness in section $z = z_5$ from: (a) model results, and (b) measurement results.

4.2. Temperature measurement

Temperature measurements were carried out using a device with a K-type thermocouple associated to a signal converter, the resulting accuracy being ± 0.2 K. Measurement points were located between the ribbon edge and the float unit wall, in the same sections where the velocity measurements were obtained.

Fig. 16 shows the model results for (a) $z = z_3$ and (b) $z = z_5$, the position of the measurement lines and the measurement points in each line. Table 2 shows the comparison between the temperature obtained by measurements and the calculated temperature from the model. With respect to the results presented in Table 2 for section $z = z_3$, experimental results show more uniform temperatures at points placed on the measurement lines y_1 and y_2 than the model results. However, the temperature differences from the model results on these lines are not very important either. Line y_3 presents nearly a uniform temperature both in the experimental results and the results from the model. On every line there are some differences between the measured and the calculated values, but the average percentage temperature difference with respect to the difference between initial and final glass temperatures is normally lower than 3%, except for line y_1, where it is 4%. Absolute average differences are lower than 10 K except for y_1, where the difference is 20 K. On the other hand, section $z = z_5$ presents similar behaviour to section $z = z_3$, though the measured results on lines y_4 and y_5 are less uniform. The temperature differences between the measurements and the model are not very great if we take into account the temperature level. As at section $z = z_3$, line

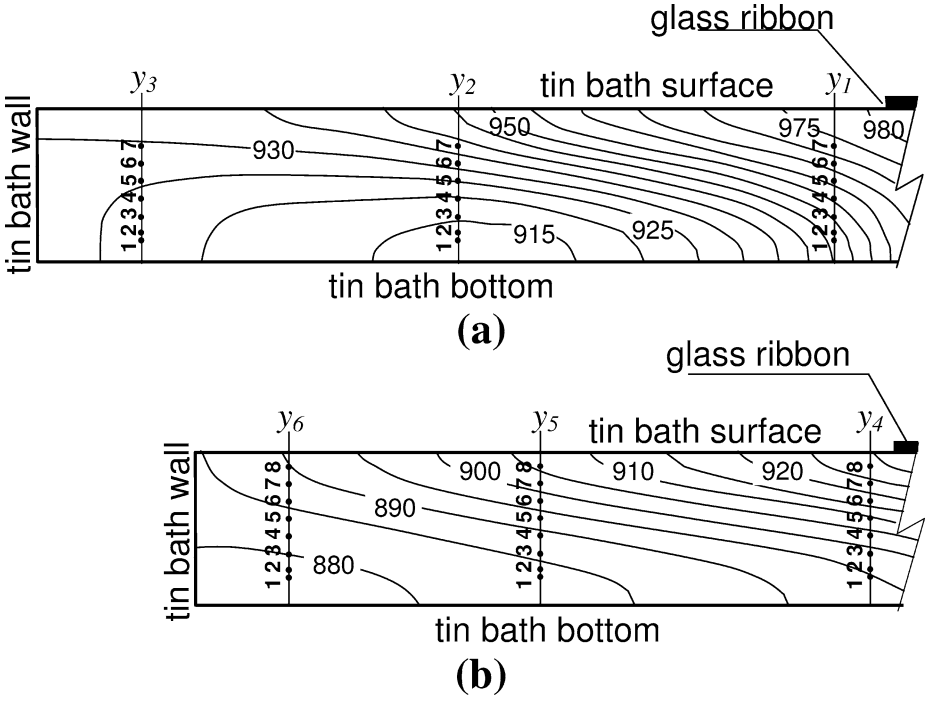

Fig. 16. Temperature contours (T, K) from the model results for a tin bath with baffles and 2 mm ribbon thickness in: (a) section $z = z_3$, and (b) section $z = z_5$. Temperature measurement positions.

Table 2
Experimental and calculated temperatures at sections $z = z_3$ and $z = z_5$

	z_3						z_5					
	y_1		y_2		y_3		y_4		y_5		y_6	
	T_e (K)	T_c (K)	T_e (K)	T_c (K)	T_e (K)	T_c (K)	T_e (K)	T_c (K)	T_e (K)	T_c (K)	T_e (K)	T_c (K)
1	936	946.0	932	912.7	932	923.6	893	894.9	–	883.5	889	879.0
2	936	947.0	933	913.5	932	923.0	893	895.2	898	884.1	889	879.6
3	936	957.5	932	916.2	932	924.5	901	898.0	898	886.0	889	880.1
4	938	956.6	932	920.0	933	924.0	901	903.5	899	889.5	889	882.0
5	938	962.0	934	925.2	933	926.2	901	910.2	900	893.2	889	883.7
6	938	968.5	934	932.1	933	928.5	901	917.0	896	899.0	889	886.0
7	935	973.0	933	938.0	932	929.0	901	924.5	893	903.5	889	888.9
8	–	–	–	–	–	–	893	927.0	888	906.8	889	890.0
$\overline{T}$	937	957.4	933	922.5	932	925.0	898	908.8	896	893.2	889	883.7
s	1.2	9.7	0.8	9.0	0.5	2.2	3.9	12.1	3.9	8.4	0.0	4.0

y_6 presents nearly an uniform temperature both in the experimental results and the results from the model. The average percentage temperature difference with respect to the difference between initial and final glass temperatures on all the lines is lower than 3%.

5. Conclusions

It has been verified both theoretically and experimentally that there exists a considerable reverse flow of tin between the vertical projection of the glass ribbon edge and the side wall of the float unit.

The reverse flow pattern depends on the use or not of baffles and the values of the velocities in the flow depend on the final ribbon thickness and increase as the thickness decreases.

For the bath without baffles, there is an important vortex under the glass ribbon with an associated important reverse flow, which diminishes in the zone where the bath gets wider because of the formation of secondary vortices between the glass ribbon edge and the vertical wall. In the narrowest zone of the bath between the glass ribbon edge projection and the float unit vertical wall, there is also an important vortex with an important reverse flow.

The use of baffles diminished the reverse flow and the temperatures gradient in the narrowest zone of the bath. The changes produced in the reverse flow velocities and in the temperatures when the glass ribbon final velocity increases, which implies that the final thickness decreases, are lower when baffles are used.

The velocity measurements and the resulting contours for the w velocity component are in good agreement with the theoretical results.

Temperature measurements are in quite good agreement with the theoretical temperatures obtained with the model. However, differences were found on the measurement lines next to the glass ribbon, which can be of up to 2%, these differences being lower than 1% on the remaining lines.

Acknowledgements

The authors would like to thank the company *Cristalería Española* (R + D Centre in Avilés) for sponsoring this research.

References

[1] L.A.B. Pilkington, The float glass process, Proc. Roy. Soc. London 314 (1969) 1–25.
[2] O.S. Narayanawamy, A one-dimensional model of stretching float glass, J. Amer. Ceramic Soc. 60 (1977) 1–5.
[3] F. Pan, A. Acrivos, Steady flows in rectangular cavities, J. Fluids Mechanics 28 (1967) 643–655.
[4] J.R. Koseff, R.L. Street, The lid-driven cavity flow: A synthesis of qualitative and quantitative observation, ASME J. Fluids Engrg. 106 (1984) 390–398.
[5] R. Siegel, J.R. Howell, Thermal Radiation Heat Transfer, Hemisphere, Washington, DC, 1992.
[6] M.M. Prieto, Fluid-dynamic and thermal study of a molten metal bath, Ph.D. Thesis, University of Oviedo, Spain, 1990.
[7] W.H. McAdams, Heat Transmission, 3rd edn., McGraw-Hill, New York, 1945.
[8] R.J. Goldstein, E.M. Sparrow, D.C. Jones, Natural convection mass transfer adjacent to the horizontal plates, Internat. J. Heat Mass Transfer 16 (1973) 1025.
[9] S.V. Patankar, Numerical Heat Transfer and Fluid Flow, Hemisphere, New York, 1980.
[10] D.B. Spalding, A general purpose computer program for multi-dimensional one- and two-phase flow, Math. Comput. Simulation XXIII (1981) 267–276.
[11] PHOENICS v2.2.2 User's Manual, CHAM Ltd. Wimbledon, United Kingdom, 1996.
[12] D.B. Spalding, Mathematical modelling of fluid-mechanics, heat-transfer and chemical-reaction processes, CFDU Report HTS/80/1, 1980.
[13] M.M. Prieto, E. Egusquiza, Development of a velocity meter for molten metals at high temperatures, in: Proceedings of Sensor '91, ACS Organisation GmbH, Wunstorf-Steinhude, Vol. 3, 1991, pp. 185–193.